

Full Quantum Dynamics Simulation of a Realistic Molecular System Using the Adaptive Time-Dependent Density Matrix Renormalization Group Method

Yao Yao

Department of Physics and State Key Laboratory of Luminescent Materials and Devices, South China University of Technology, Guangzhou 510640, China

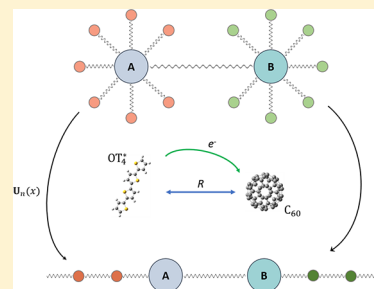
Ke-Wei Sun

School of Science, Hangzhou Dianzi University, Hangzhou 310018, China

Zhen Luo and Haibo Ma*^{id}

Key Laboratory of Mesoscopic Chemistry of MOE, School of Chemistry and Chemical Engineering, Nanjing University, Nanjing 210023, China

ABSTRACT: The accurate theoretical interpretation of ultrafast time-resolved spectroscopy experiments relies on full quantum dynamics simulations for the investigated system, which is nevertheless computationally prohibitive for realistic molecular systems with a large number of electronic and/or vibrational degrees of freedom. In this work, we propose a unitary transformation approach for realistic vibronic Hamiltonians, which can be coped with using the adaptive time-dependent density matrix renormalization group (t-DMRG) method to efficiently evolve the nonadiabatic dynamics of a large molecular system. We demonstrate the accuracy and efficiency of this approach with an example of simulating the exciton dissociation process within an oligothiophene/fullerene heterojunction, indicating that t-DMRG can be a promising method for full quantum dynamics simulation in large chemical systems. Moreover, it is also shown that the proper vibronic features in the ultrafast electronic process can be obtained by simulating the two-dimensional (2D) electronic spectrum by virtue of the high computational efficiency of the t-DMRG method.



Thanks to the recent advancements of time-resolved spectroscopy technology, nowadays a lot of ultrafast excited-state processes within the time scale of 10s to 100s of femtoseconds, and nonadiabatic phenomena caused by the crossing of potential energy surfaces have been observed in a large number of systems ranging from biological ones^{1,2} to gaseous and condensed-phase materials.^{3,4} Theoretical understanding of these ultrafast nonadiabatic processes can be achieved via a solution of the quantum dynamics of the molecular systems; however, such a kind of solution for the dynamics involving the electron–nuclear couplings is nontrivial and requires breaking the Born–Oppenheimer approximation, which is one of the basic assumptions in quantum chemistry. To overcome this great difficulty, in the recent years, many dynamics methodologies have been proposed, including full quantum methods (multi-configuration time-dependent Hartree (MCTDH) approach⁵ and its multilayer version (ML-MCTDH),⁶ quasi-adiabatic path integral (QUAPI),⁷ full multiple spawning (FMS),⁸ etc.), semi-classical methods (Ehrenfest mean-field approach,⁹ surface hopping method,^{9,10} etc.), and quantum dissipation approaches (Redfield theory,¹¹ hierarchical equations of motion (HEOM) method,¹² various stochastic differential equation methods^{13,14}).

Nevertheless, the full quantum dynamics simulation for systems with a large number of quantum degrees of freedom is currently still a great challenge due to the expensive increase of computational costs with increasing system size.

The density matrix renormalization group (DMRG) method proposed by White in 1992¹⁵ is a promising tool for dealing with strongly coupled electronic–vibrational systems, which has been shown to be an extremely accurate numerical technique in solving one-dimensional (1D) strongly correlated systems.^{16–19} Only a fixed number (M) of renormalized states during enlargement of the system is kept in DMRG by using the eigenvalues of the subsystem's reduced density matrix as the decimation criterion of the Hilbert space. Therefore, DMRG has been successfully applied to the solution of 1D Hamiltonians with large size. The application of DMRG was later extended to simulate the dynamics of 1D electronic and bosonic systems with high computational accuracy and efficiency by using an adaptive

Received: December 5, 2017

Accepted: January 3, 2018

Published: January 3, 2018

time-dependent DMRG (t-DMRG) approach^{20–22} based on Vidal's time-evolving block-decimation (TEBD) algorithm,^{23,24} for example, in the context of spin-charge separation in cold Fermi gases,²⁵ dynamical quasicondensation of hard-core Bosons at finite momenta,²⁶ and far-from-equilibrium properties of interacting nanostructures.²⁷ Unfortunately, the adaptive t-DMRG cannot be applied straightforward to general vibronic Hamiltonians that do not have a 1D representation because the prerequisite for using the adaptive t-DMRG is that the Hamiltonian operator \hat{H} of the total system can be decomposed into local terms \hat{h}_n that live only on neighboring sites n and $n + 1$.

t-DMRG can be also reformulated using the language of the matrix product state (MPS)^{28–30} and matrix product operator (MPO).^{31,32} Haegeman et al.^{33,34} and Zaletel et al.³⁵ recently suggested that the MPS representation of the t-DMRG wave function can be adapted for arbitrary Hamiltonians, on the basis of the time-dependent variational principle (TDVP)^{36,37} or some kind of approximation in terms of MPO. Another efficient way to simulate the nonadiabatic dynamics with the adaptive t-DMRG for general vibronic Hamiltonians is to transform vibronic Hamiltonian \hat{H} into an effective 1D representation. Such a kind of transformation has been partly achieved via mapping between system–reservoir quantum models and semi-infinite discrete chains using orthogonal polynomials³⁸ for spin-boson models^{39,40} and other model Hamiltonians⁴¹ that use a continuous phonon spectrum and the uniform vibronic coupling parameters for different electronic states.

The application of t-DMRG to photophysical dynamics simulations of realistic molecules comprising a discretized phonon spectrum is naturally motivated but not reported yet. On one hand, the light-harvesting systems in biological or condensed-phase material systems always have many excitonic states, making the excitons and phonons complexly entangled with each other.^{42,43} On the other hand, both the diagonal and off-diagonal vibronic couplings are present in many organic molecules, making the dynamics sensitive to the parameters.^{44,45} These facts make the vibronic Hamiltonian in these systems not a DMRG-friendly 1D representation with only nearest-neighbor interactions, and accordingly, the direct implementation of the adaptive t-DMRG to realistic molecular systems becomes infeasible.

In order to overcome the above difficulty, in this work, we propose a unitary transformation approach for realistic vibronic Hamiltonians, which can be efficiently coped with using the adaptive t-DMRG method to evolve the nonadiabatic dynamics of a large molecular system. As a starting point to examine whether t-DMRG could be successfully applied to the realistic molecules, one has to utilize a well-established but nontrivial model system as the instance. In this context, we present our t-DMRG algorithm to study the ultrafast exciton dissociation dynamics at the organic donor/acceptor (oligothiophene/fullerene) heterojunction, which is a crucial step in the optoelectronic conversion processes in organic solar cells and has been recently simulated by various other quantum dynamics methods including MCTDH and HEOM.^{46–49}

The adaptive t-DMRG method^{20–22} is an efficient numerical method to solve the time-dependent Schrödinger equation

$$\hat{H}\Psi(t) = i\hbar \frac{\partial \Psi(t)}{\partial t}$$

$$\Psi(t + \Delta t) = \hat{U}(\Delta t)\Psi(t) \text{ with } \hat{U}(\Delta t) = \exp(-i\hat{H}\Delta t/\hbar) \quad (1)$$

Dynamics simulation in the adaptive t-DMRG is based on the Trotter–Suzuki decomposition of the time-evolution operator $\hat{U}(\Delta t)$ of eq 1. If the Hamiltonian of the 1D system is a summation of local terms \hat{h}_n that live only on neighboring sites n and $n + 1$, i.e.

$$\hat{H} = \sum_n \hat{h}_n \quad (2)$$

$\hat{U}(\Delta t)$ can be approximated by an n th-order Trotter–Suzuki decomposition,^{50,51} e.g., to second order

$$\hat{U}(\Delta t) = \prod_{n \in \text{even}} \hat{U}_n(\Delta t/2) \prod_{n \in \text{odd}} \hat{U}_n(\Delta t) \prod_{n \in \text{even}} \hat{U}_n(\Delta t/2) + O(\Delta t^3) \quad (3)$$

$\hat{U}_n(\Delta t)$ is the infinitesimal time-evolution operator $\exp(-i\hat{h}_n(t)\Delta t/\hbar)$, which only applies to nearest-neighbor sites n and $n + 1$ in the 1D chain. It should be mentioned that “even” and “odd” operators commute among themselves and accordingly the ordering within the even or odd products does not matter. Then one can apply these operators $\hat{U}_n(\Delta t)$ successively to some state $|\psi\rangle$ into finite-system DMRG sweeps.^{15,16} Each operator $\hat{U}_n(\Delta t)$ is applied at a finite-system DMRG step with sites n and $n + 1$ being the active sites, i.e., where sites n and $n + 1$ are represented without truncation. For example, in an L -site 1D chain, at a finite-system DMRG step with n and $n + 1$ being the active sites, we can use eq 4 to describe a DMRG state in the form of MPS

$$|\psi\rangle = \sum_{\sigma_1}^N \dots \sum_{\sigma_L}^N A^1[\sigma_1]A^2[\sigma_2]\dots A^L[\sigma_L]|\sigma_1 \dots \sigma_L\rangle \quad (4)$$

where $\{|\sigma_i\rangle\}$ denotes the state space of dimension N for site i , matrices A^i with the dimension $M \times M$ are for site i , and the first and last A matrices are taken to be row and column vectors. Then, it is easy to describe the new state after the operation of $\hat{U}_n(\Delta t)$

$$\hat{U}_n(\Delta t)|\psi\rangle = \sum_{\sigma'_n \sigma'_{n+1}} \sum_{\sigma_1 \dots \sigma_L} \hat{U}_n(\Delta t)_{\sigma'_n \sigma'_{n+1}, \sigma_n \sigma_{n+1}} A^1[\sigma_1] \dots A^n[\sigma'_n] A^{n+1}[\sigma'_{n+1}] \dots A^L[\sigma_L] |\sigma_1 \dots \sigma'_n \sigma'_{n+1} \dots \sigma_L\rangle \quad (5)$$

without any additional error because $\hat{U}_n(\Delta t)$ acts only on the part of Hilbert space $(|\sigma_n\rangle|\sigma_{n+1}\rangle)$ with the dimension N^2 , which is exactly represented. Similar to conventional DMRG, in order to prevent exponential growth of the matrix dimension for continuing the finite-system sweep, DMRG truncations from $N \times M$ to M must be carried out. However, differently, the adaptive t-DMRG uses $\hat{U}_n(\Delta t)|\Psi\rangle$ as the target state instead of $|\Psi\rangle$ to build the reduced density matrix. After all of the local time-evolution operators at different sites have been applied successively to $\Psi(t)$ within a few sweeps, one can get the wave function $\Psi(t + \Delta t)$ for the new time $t + \Delta t$ and continue to longer times. More technical details about t-DMRG can be found in refs 20–22.

From the above introduction to the adaptive t-DMRG, one can notice that the Hamiltonian of the total system \hat{H} can be described by a sum of local terms \hat{h}_n acting only on neighboring sites n and $n + 1$ ($\hat{H} = \sum_n \hat{h}_n$) and is a mandatory prerequisite for performing the adaptive t-DMRG simulations. However, the general vibronic Hamiltonian in realistic molecules does not fulfill this requirement. In a Frenkel exciton (XT)–charge transfer (CT) mixing model in organic heterojunctions, e.g., we have to consider a system of two diabatic electronic states coupled with f vibrational modes ($\hbar = 1$)

$$\begin{aligned}\hat{H} &= \hat{H}_1 + \hat{H}_2 \\ \hat{H}_1 &= \begin{pmatrix} -\Delta & V \\ V & \Delta \end{pmatrix} \\ \hat{H}_2 &= \sum_{\nu=1}^f \omega_{\nu} \hat{a}_{\nu}^{\dagger} \hat{a}_{\nu} + \sum_{\nu=1}^f \begin{pmatrix} x_{\nu} & 0 \\ 0 & y_{\nu} \end{pmatrix} \hat{a}_{\nu} + \begin{pmatrix} x_{\nu}^{*} & 0 \\ 0 & y_{\nu}^{*} \end{pmatrix} \hat{a}_{\nu}^{\dagger}\end{aligned}\quad (6)$$

where $\hat{a}_{\nu}^{\dagger}(\hat{a}_{\nu})$ is the creation (annihilation) operator of the phonon of the ν th vibrational mode, ω_{ν} being the associated vibrational frequency, and 2Δ and V are the energy separation between the two diabatic excitonic states at the origin of the nuclear coordinate space and electronic interaction between these two states, respectively. The sets x_{ν} and y_{ν} represent the linear vibronic coupling strength parameters of relevant excitonic state. Here, for simplicity, we do not consider the off-diagonal vibronic coupling. Obviously, this realistic Hamiltonian in eq 6 does not meet the requirement of eq 2 (see Figure 1a). Normally for a spin-boson model, it is quite straightforward to transform the independent bare phonons into some semi-infinite chain by unitary transformation.³⁹ In the realistic case, however, the coupling strengths for different excitonic states and phonon modes are different, making the common transformation invalid, although the vibronic coupling model including both diagonal and off-diagonal couplings has been shown to be able to be transformed to an equivalent band-diagonal chain (but not a t-DMRG-friendly tridiagonal form).^{52,53} To this end, we transform \hat{H}_2 as the following form⁵⁴

$$\begin{aligned}\hat{H}_2 &= \sum_{\nu=1}^f \omega_{\nu} \hat{a}_{\nu}^{\dagger} \hat{a}_{\nu} + \hat{C} \sum_{\nu=1}^f c_{\nu} (\hat{Q}_{\nu} \hat{a}_{\nu} + \hat{Q}_{\nu}^{\dagger} \hat{a}_{\nu}^{\dagger}) \\ &+ \sum_{\nu=1}^f r_{\nu} (\hat{Q}_{\nu} \hat{a}_{\nu} + \hat{Q}_{\nu}^{\dagger} \hat{a}_{\nu}^{\dagger})\end{aligned}\quad (7)$$

$$\begin{aligned}\hat{H}_2 &= \sum_{\nu=1}^f \omega_{\nu} \hat{a}_{\nu}^{\dagger} \hat{a}_{\nu} + \hat{C} \sum_{\nu=1}^f c_{\nu} (\hat{a}_{\nu} + \hat{a}_{\nu}^{\dagger}) + \sum_{\nu=1}^f r_{\nu} (\hat{a}_{\nu} + \hat{a}_{\nu}^{\dagger}) \\ &= \sum_{\nu=1}^f \omega_{\nu} \left(\hat{a}_{\nu}^{\dagger} + \frac{r_{\nu}}{\omega_{\nu}} \right) \left(\hat{a}_{\nu} + \frac{r_{\nu}}{\omega_{\nu}} \right) + \hat{C} \sum_{\nu=1}^f c_{\nu} \left[\left(\hat{a}_{\nu}^{\dagger} + \frac{r_{\nu}}{\omega_{\nu}} \right) + \left(\hat{a}_{\nu} + \frac{r_{\nu}}{\omega_{\nu}} \right) \right] - \hat{S}\end{aligned}\quad (8)$$

where $\hat{S} \equiv \sum_{\nu=1}^f (r_{\nu}^2/\omega_{\nu}) + \hat{C} \sum_{\nu=1}^f (c_{\nu} r_{\nu}^2/\omega_{\nu}^2)$ merely acts on the excitonic states and could be absorbed into \hat{H}_1 . Let us write \hat{H}_2 in a more compact form by defining $\hat{b}_{\nu} \equiv \hat{a}_{\nu} + (r_{\nu}/\omega_{\nu})$, and the final form reads

$$\hat{H}_2 = \hat{H}_2 + \hat{S} = \sum_{\nu=1}^f \omega_{\nu} \hat{b}_{\nu}^{\dagger} \hat{b}_{\nu} + \hat{C} \sum_{\nu=1}^f c_{\nu} (\hat{b}_{\nu} + \hat{b}_{\nu}^{\dagger})\quad (9)$$

We finally obtain a compact form that could be unitarily transformed into a semi-infinite bosonic chain with the Hamiltonian being

$$\hat{H}_2 = \sum_i [\epsilon_i \hat{b}_i^{\dagger} \hat{b}_i + t_i (\hat{b}_{i+1}^{\dagger} \hat{b}_i + \text{h.c.})] + \gamma \hat{C} (\hat{b}_1 + \hat{b}_1^{\dagger})\quad (10)$$

Following the standard procedure in the numerical renormalization group,⁵⁵ we define a unitary matrix $U_{i,\nu}$ to transform \hat{b}_{ν} to \hat{b}_i . The parameters are subsequently obtained by the following formula

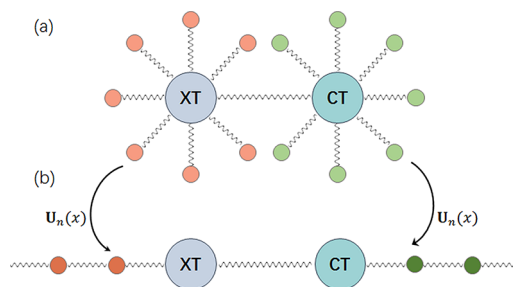


Figure 1. (a) The standard Hamiltonian has electronic states (XT and CT) interacting with their surrounding bosonic phonon bath of two molecules in a starlike configuration. (b) After a unitary transformation of the bosonic modes only for each molecule, a 1D chain Hamiltonian with only nearest-neighbor couplings can be generated from two semichains.

where we have made $\hat{R}_{\nu} \equiv \begin{pmatrix} x_{\nu} & 0 \\ 0 & y_{\nu} \end{pmatrix}$ equal to $(c_{\nu} \hat{C} + r_{\nu} \hat{I}) \hat{Q}_{\nu}$, which is similar to a mass-center transformation for the excitons, with \hat{I} being the identity matrix, \hat{C} being Hermitian, and c_{ν} and r_{ν} being combination coefficients. Herein, if we appropriately set the operator \hat{C} and the combination coefficients, it is quite possible to obtain a series of operators \hat{Q}_{ν} that satisfy $\hat{Q}_{\nu}^{\dagger} \hat{Q}_{\nu} = \hat{Q}_{\nu} \hat{Q}_{\nu}^{\dagger} = \hat{I}$. For example, in our two-level excitonic system without off-diagonal couplings, \hat{C} is naturally chosen to be $\begin{pmatrix} 1 & 0 \\ 0 & 0 \end{pmatrix}$ and $c_{\nu} = x_{\nu} - y_{\nu}$, $r_{\nu} = y_{\nu}$; therefore, the operator \hat{Q}_{ν} equals to the identity matrix.

Taking the commutation relation of \hat{Q}_{ν} into consideration, we can rationally define another bosonic operator $\hat{a}_{\nu} \equiv \hat{Q}_{\nu} \hat{a}_{\nu}$. The Hamiltonian (eq 7) could be rewritten as

$$\begin{aligned}\gamma^2 &= \sum_{\nu=1}^f c_{\nu}^2 & \epsilon_i &= \sum_{\nu=1}^f \omega_{\nu} U_{i,\nu}^2 \\ t_i^2 &= \sum_{\nu=1}^f [(\omega_{\nu} - \epsilon_i) U_{i,\nu} - t_{i-1} U_{i-1,\nu}]^2 \quad (t_0 = 0) \\ U_{0,\nu} &= \frac{c_{\nu}}{\sqrt{\gamma}} & U_{1,\nu} &= \frac{\omega_{\nu} - \epsilon_0}{t_0} U_{0,\nu} \\ U_{i+1,\nu} &= \frac{1}{t_i} [(\omega_{\nu} - \epsilon_i) U_{i,\nu} - t_{i-1} U_{i-1,\nu}]\end{aligned}\quad (11)$$

In the following, we take a benchmark model system, the oligothiophene (OT)–fullerene (C_{60}) interface, as an instance to investigate the applicability of t-DMRG on the realistic molecular system. The thiophene is one of the most used donor molecules due to its optimal opto- and electroproperties. The fullerene dominated the battles of acceptor molecules for many years until recently the nonfullerene acceptors⁵⁶ came into play. In our simulation, the energy and coupling parameters for XT and CT diabatic states are taken from Table 1 of ref 48, and the vibrational

frequencies and electron–phonon coupling strengths are extracted from Figure 2b of ref 47.

Figure 2a shows the time evolution of population for four sets of parameters of local phonon number P and the number of preserved states M in DMRG truncation. The curves of $P = 6$, $M = 64$ for $R = 0.3$ nm could be straightforwardly compared with Figure 5 of ref 48 and Figure 4 of ref 47, which were obtained by the MCTDH method. One can find that, up to 250 fs, the population evolution exhibits perfect agreement with that from MCTDH, which could be recognized as accurate because the absorption spectrum computed via the dynamics results has been explicitly compared with the experimental measurement. The comparison between t-DMRG and MCTDH figures out the consistency that the two methods make up for the realistic thiophene/fullerene interface. For t-DMRG, the consuming resource of computation is rather reasonable. Our test program is not parallelized and did not even run on the workstation, but for one curve, it takes fewer than 10 computing hours on a normal laptop.

We study the convergence of our results by changing both P and M . It is found that by changing P from 3 to 6 the curves change in a visible manner. To be specific, the curves of $P = 3$ and 6 diverge at 20 fs, which means that $P = 3$ fails to capture the correct dynamics. Regardless of the detailed difference, the curve of $P = 4$ approximately matches that of $P = 6$ until 100 fs. We have also compared $P = 6$ and 8 (not shown), and the results are much closer than that in the above cases. As a result, for the parameters in the present system, $P = 6$ is an optimal value for the local phonons. More importantly, one can see from the inset of Figure 2a that the truncation number M does not completely matter in the present calculations. This is essential because in a practical computation one can reduce M to as small as possible to minimize the computing time without losing accuracy.

As we are studying a donor/acceptor heterojunction structure, the phonon modes are obviously separated in each layer. One would consider that in other realistic systems phonons in the two layers must be dealt with separately (e.g., in the case of energy transfer from the donor to acceptor). In other numerical methods, the phonons are always treated in a mixed manner, but t-DMRG has the advantage that the excitonic site could be connected with two independent semi-infinite bosonic lattices,

allowing us to separate the phonons in the donor and acceptor into two lattices (shown in Figure 1). Figure 2b shows the results, merely considering the phonons in the donor or acceptor. As the number of phonon modes decreases, the population evolution shows stronger oscillation than that considering phonons in both layers simultaneously.

Quantum coherence of excitons at the P3HT/PCBM interface has been extensively investigated by ultrafast optics. Intuitively, the shorter the distance between donor and acceptor molecules, the larger the coupling between the local exciton and CT state, and thus the stronger the coherence. Figure 3 shows the evolution of population and coherence for $R = 0.25, 0.3$, and 0.35 nm. The population of $R = 0.3$ nm decreases quickly before 35 fs and then oscillates around a mean value of about 0.2, indicating that the charge transfer process is efficient and the steady value is achieved on an ultrafast time scale. It is obvious that for the short distance the oscillation of both the population and coherence is much stronger than those of longer distance. Interestingly, however, one can find the real components of coherence of $R = 0.3$ and 0.35 nm have a finite value while the coherence of $R = 0.25$ nm oscillates around zero. This is because the electronic interactions between XT and CT states are too strong such that the vibronic coupling can not be responsible. It could make sense from our model Hamiltonian that the XT–CT coherence could have a nonvanishing average value as long as the phonon modes have finite displacement. When the vibronic coupling is negligible compared with the electronic interaction, this mechanism does not work so that the average coherence vanishes for $R = 0.25$ nm. As a result, the average value of the exciton population for $R = 0.25$ nm is surprisingly larger than that for $R = 0.3$ nm in the time extent of our computations. This implies that the short distance does not benefit the charge transfer and thus the charge separation in this system.

To our knowledge, so far, there is no simulations of the two-dimensional (2D) coherent electronic spectroscopy using the t-DMRG algorithm. As shown above, t-DMRG produces promising dynamical results for the OT₄/C₆₀ interface, so that it is intuitive to use t-DMRG to study the 2D spectrum, which is nothing but the third-order nonlinear response function R_i , $i = 1 \rightarrow 4$, written as^{57–59}

$$\begin{aligned}
 R_1(\tau, T, t) &= \left(\frac{i}{\hbar}\right)^3 \theta(t)\theta(T)\theta(\tau) \sum_{e_4 e_3 e_2 e_1} \mu_{ge_4} \mu_{e_3g} \mu_{ge_1} \mu_{e_2g} \mathbf{G}_{e_2g, e_2g}(t) \mathbf{G}_{e_4g, e_4g}(\tau) \mathbf{G}_{e_4e_3, e_2e_1}(T) \\
 R_2(\tau, T, t) &= \left(\frac{i}{\hbar}\right)^3 \theta(t)\theta(T)\theta(\tau) \sum_{e_4 e_3 e_2 e_1} \mu_{ge_4} \mu_{e_3g} \mu_{e_2g} \mu_{ge_1} \mathbf{G}_{ge_1, ge_1}(t) \mathbf{G}_{e_4g, e_4g}(\tau) \mathbf{G}_{e_4e_3, e_2e_1}(T) \\
 R_3(\tau, T, t) &= \left(\frac{i}{\hbar}\right)^3 \theta(t)\theta(T)\theta(\tau) \sum_{e_4 e_1} \mu_{ge_4} \mu_{e_4g} \mu_{e_1g} \mu_{ge_1} \mathbf{G}_{ge_1, ge_1}(t) \mathbf{G}_{e_4g, e_4g}(\tau) \\
 R_4(\tau, T, t) &= \left(\frac{i}{\hbar}\right)^3 \theta(t)\theta(T)\theta(\tau) \sum_{e_4 e_2} \mu_{ge_4} \mu_{e_4g} \mu_{ge_2} \mu_{e_2g} \mathbf{G}_{e_2g, e_2g}(t) \mathbf{G}_{e_4g, e_4g}(\tau)
 \end{aligned} \tag{12}$$

where the dipole operator μ_{eg} means the transitions from the ground state g to the excited-state manifold e , and $\mu_{ge} = \mu_{eg}^* = 1$ for bright states and 0 for dark states. In eq 12, we have used a tetradic Green's function, including the ground-state and the excited-state manifold, to represent both coherence and population relaxation, that is

$$\rho_{i_4 i_3}(t) = \sum_{i_2 i_1} \mathbf{G}_{i_4 i_3, i_2 i_1}(t) \rho_{i_2 i_1}(0) \tag{13}$$

where $i_k = g, e$. In order to calculate all of the Green's functions, it is necessary to calculate the dynamics of the system with the initial states being $|g\rangle\langle g|$, $|e\rangle\langle e|$, $|g\rangle\langle e|$, $|e\rangle\langle g|$. The former two

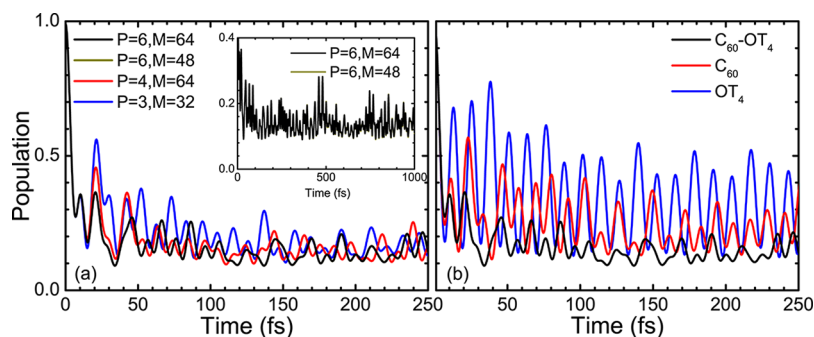


Figure 2. (a) Population evolution for four sets of numbers of local phonon mode P and truncation number of states in reduced density matrix M . (b) Population evolution for three cases: Simultaneously taking phonons in both OT_4 and C_{60} into account and only considering phonons in OT_4 and C_{60} individually. For all curves, R is set to 0.3 nm.

could be easily computed by t-DMRG with the normal procedure. For the latter two states, we can alternatively calculate the dynamics with initial states being $(|g\rangle \pm |e\rangle)/\sqrt{2}$ and make a simple linear combination to obtain all of the dynamical results that we want. With these results in hand, it is thus applicable to calculate the 2D spectrum in a credible manner. The rephasing (R) and nonrephasing (NR) 2D photon-echo spectra are subsequently evaluated by 2D Fourier transforms as^{57–59}

$$S_R(\omega_\tau, T, \omega_t) = \text{Re} \int_0^\infty \int_0^\infty d\tau dt i(R_2(\tau, T, t) + R_3(\tau, T, t))e^{-i\omega_\tau t + i\omega_t \tau} \quad (14)$$

$$S_{NR}(\omega_\tau, T, \omega_t) = \text{Re} \int_0^\infty \int_0^\infty d\tau dt i(R_1(\tau, T, t) + R_4(\tau, T, t))e^{i\omega_\tau t + i\omega_t \tau} \quad (15)$$

The total 2D spectrum is then defined by the sum of the two

$$S(\omega_\tau, T, \omega_t) = S_R(\omega_\tau, T, \omega_t) + S_{NR}(\omega_\tau, T, \omega_t) \quad (16)$$

Figure 4a displays the real part of the 2D spectrum at the waiting time $T = 0$. A main positive diagonal peak that arises from the zero phonon transition occurs at around $(\omega_t = -0.08 \text{ eV}, \omega_\tau = -0.08 \text{ eV})$, which emerges from the absorption and the emission between the ground state and the bright excited state. The red shift is present due to the coupling between the system and the vibrational modes. The perfectly symmetric off-diagonal peaks show the feature of the two-level system, and some pronounced vibrational structures are obviously observed. In order to see these vibrational structures more clearly, the linear absorption spectrum is obtained by extracting the diagonal values of the 2D spectrum, as shown in Figure 4b. A main peak stemming from the 0–0 transition can be found, which exhibits a Gaussian line shape rather than a Lorentzian line shape. The Gaussian line shape without spectrum diffusion arises from the coherent dynamics, implying that the t-DMRG dynamics holds the vibronic coherence very well. Moreover, there are two visible vibrational side peaks located at around 0.092 and 0.31 eV. The first side peak at 0.092 eV stemming from the 0 to 1 transition corresponds to the main vibrational modes that concentrate at around 0.2 eV (1585 cm^{-1}).⁴⁷ The second side peak at 0.31 eV is from multiphonon absorption. Consequently, our 2D spectrum calculation has achieved the major vibronic features of the OT_4/C_{60} interface, implying that the t-DMRG algorithm is available to

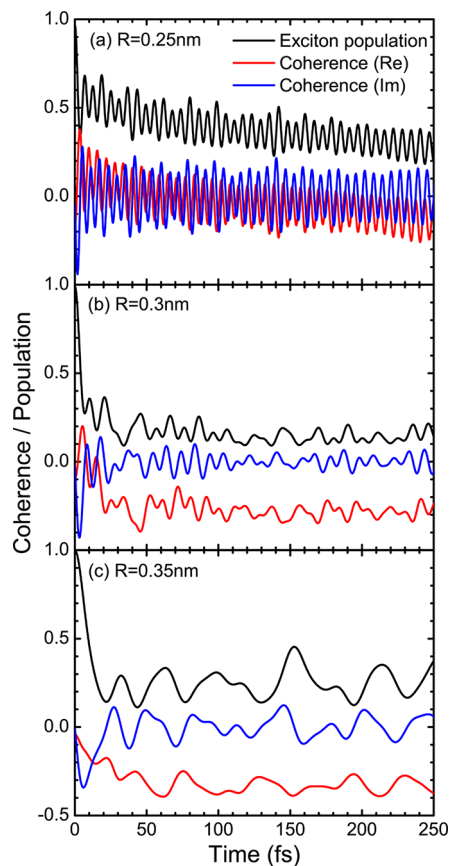


Figure 3. Evolution of population of the XT state and coherence between XT and CT states for R equal to (a) 0.3, (b) 0.25, and (c) 0.35 nm.

compute the multidimensional coherent spectra for the realistic systems.

In summary, we have adopted a unitary transformation for the t-DMRG to deal with a realistic system, namely, the oligothiophene/fullerene interface. Our dynamical results exhibit promising accuracy and efficiency compared with that from the MCTDH method. It is found that as the interfacial distance becomes shorter the quantum coherence tends to be stronger, but conversely, the charge transfer tends to be weaker. The 2D coherent electronic spectrum is for the first time simulated by the t-DMRG method, and the vibronic feature of the exciton dissociation is captured in a credible manner. For future extension, it is suggested to combine the t-DMRG method with

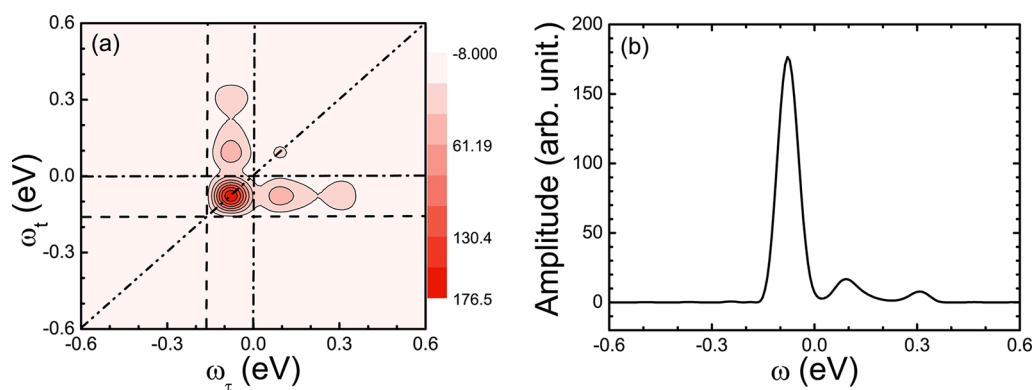


Figure 4. (a) 2D spectrum of the OT₄/C₆₀ for $R = 0.3$ nm. The dashed lines indicate the energy of the CT state, while the dashed–dotted line is for the XT state. The dashed–dotted–dotted line signifies the diagonal line with $\omega_t = \omega_\tau$. (b) Linear absorption spectrum extracted from the diagonal line.

the thermo-field-dynamics approach⁶⁰ to get the finite-temperature effect so that the calculated dynamics and the optical spectra are closer to the realistic situation.

AUTHOR INFORMATION

Corresponding Author

*E-mail: haibo@nju.edu.cn.

ORCID

Haibo Ma: 0000-0001-7915-3429

Notes

The authors declare no competing financial interest.

ACKNOWLEDGMENTS

The work was supported by the National Natural Science Foundation of China [Grant Numbers 21673109, 21722302, 91333202, 11574052, and 11404084]. We thank Prof. Michèle Desouter-Lecomte for valuable discussions.

REFERENCES

- Romero, E.; Augulis, R.; Novoderezhkin, V. I.; Ferretti, M.; Thieme, J.; Zigmantas, D.; van Grondelle, R. Quantum Coherence in Photosynthesis for Efficient Solar-Energy Conversion. *Nat. Phys.* **2014**, *10*, 676–682.
- Lambert, N.; Chen, Y.; Cheng, Y.; Li, C.; Chen, G.; Nori, F. Quantum Biology. *Nat. Phys.* **2013**, *9*, 10–18.
- Gélinas, S.; Rao, A.; Kumar, A.; Smith, S. L.; Chin, A. W.; Clark, J.; van der Poll, T. S.; Bazan, G. C.; Friend, R. H. Ultrafast Long-Range Charge Separation in Organic Semiconductor Photovoltaic Diodes. *Science* **2014**, *343*, 512–516.
- Falke, S. M.; Rozzi, C. A.; Brida, D.; Maiuri, M.; Amato, M.; Sommer, E.; De Sio, A.; Rubio, A.; Cerullo, G.; Molinari, E.; Lienau, C. Coherent Ultrafast Charge Transfer in an Organic Photovoltaic Blend. *Science* **2014**, *344*, 1001–1005.
- Beck, M. H.; Jackle, A.; Worth, G. A.; Meyer, H. D. The Multiconfiguration Time-Dependent Hartree (MCTDH) Method: a Highly Efficient Algorithm for Propagating Wavepackets. *Phys. Rep.* **2000**, *324*, 1–105.
- Wang, H. B.; Thoss, M. Multilayer Formulation of the Multiconfiguration Time-Dependent Hartree Theory. *J. Chem. Phys.* **2003**, *119*, 1289–1299.
- Makri, N.; Makarov, D. E. Tensor Propagator for Iterative Quantum Time Evolution of Reduced Density Matrices. I. Theory. *J. Chem. Phys.* **1995**, *102*, 4600–4610.
- Martinez, T. J.; Ben-Nun, M.; Levine, R. D. Multi-Electronic-State Molecular Dynamics: a Wave Function Approach with Applications. *J. Phys. Chem.* **1996**, *100*, 7884–7895.
- Tully, J. C. Mixed Quantum-Classical Dynamics. *Faraday Discuss.* **1998**, *110*, 407–419.
- Wang, L.; Akimov, A.; Prezhdo, O. V. Recent Progress in Surface Hopping: 2011–2015. *J. Phys. Chem. Lett.* **2016**, *7*, 2100–2112.
- Redfield, A. G. On the Theory of Relaxation Processes. *IBM J. Res. Dev.* **1957**, *1*, 19–31.
- Tanimura, Y.; Kubo, R. Time Evolution of a Quantum System in contact with a Nearly Gaussian-Markoffian Noise Bath. *J. Phys. Soc. Jpn.* **1989**, *58*, 101–114.
- Han, L.; Zhong, X.; Liang, W.; Zhao, Y. Energy relaxation and separation of a hot electron-hole pair in organic aggregates from a time-dependent wavepacket diffusion method. *J. Chem. Phys.* **2014**, *140*, 214107.
- Yan, Y.; Shao, J. Stochastic description of quantum Brownian dynamics. *Front. Phys.* **2016**, *11*, 110309.
- White, S. R. Density Matrix Formulation for Quantum Renormalization Groups. *Phys. Rev. Lett.* **1992**, *69*, 2863–2866.
- Schollwöck, U. The Density-Matrix Renormalization Group. *Rev. Mod. Phys.* **2005**, *77*, 259–315.
- Hallberg, K. Numerical Methods for Nanoscopic Systems Based on Density Matrix Renormalization. *J. Comput. Theor. Nanosci.* **2008**, *5*, 923.
- Schollwöck, U. The Density-Matrix Renormalization Group in the age of Matrix Product States. *Ann. Phys.* **2011**, *326*, 96–192.
- Schollwöck, U. The Density-Matrix Renormalization Group: a Short Introduction. *Philos. Trans. R. Soc., A* **2011**, *369*, 2643–2661.
- White, S. R.; Feiguin, A. Real-Time Evolution Using the Density Matrix Renormalization Group. *Phys. Rev. Lett.* **2004**, *93*, 076401.
- Daley, A. J.; Kollath, C.; Schollwöck, U.; Vidal, G. Time-Dependent Density-Matrix Renormalization Group Using Adaptive Effective Hilbert Spaces. *J. Stat. Mech.: Theory Exp.* **2004**, *2004*, P04005.
- Ma, H.; Luo, Z.; Yao, Y. The time-dependent density matrix renormalisation group method. *Mol. Phys.* **2018**, DOI: 10.1080/00268976.2017.1406165.
- Vidal, G. Efficient Classical Simulation of Slightly Entangled Quantum Computations. *Phys. Rev. Lett.* **2003**, *91*, 147902.
- Vidal, G. Efficient Simulation of One-Dimensional Quantum Many-Body Systems. *Phys. Rev. Lett.* **2004**, *93*, 040502.
- Kollath, C.; Schollwöck, U.; Zwirger, W. Spin-Charge Separation in Cold Fermi Gases: a Real Time Analysis. *Phys. Rev. Lett.* **2005**, *95*, 176401.
- Vidmar, L.; Ronzheimer, J. P.; Schreiber, M.; Braun, S.; Hodgman, S. S.; Langer, S.; Heidrich-Meisner, F.; Bloch, I.; Schneider, U. Dynamical Quasicondensation of Hard-Core Bosons at Finite Momenta. *Phys. Rev. Lett.* **2015**, *115*, 175301.
- Boulat, E.; Saleur, H.; Schmitteckert, P. Twofold Advance in the Theoretical Understanding of Far-from-Equilibrium Properties of Interacting Nanostructures. *Phys. Rev. Lett.* **2008**, *101*, 140601.
- Fannes, M.; Nachtergaele, B.; Werner, R. F. Finitely Correlated States on Quantum Spin Chains. *Commun. Math. Phys.* **1992**, *144*, 443–490.
- Östlund, S.; Rommer, S. Thermodynamic Limit of Density Matrix Renormalization. *Phys. Rev. Lett.* **1995**, *75*, 3537.

- (30) Rommer, S.; Östlund, S. Class of Ansatz Wave Functions for One-Dimensional Spin Systems and Their Relation to the Density Matrix Renormalization Group. *Phys. Rev. B: Condens. Matter Mater. Phys.* **1997**, *55*, 2164–2181.
- (31) McCulloch, I. P. From Density-Matrix Renormalization Group to Matrix Product States. *J. Stat. Mech.: Theory Exp.* **2007**, *2007*, P10014.
- (32) Pirvu, B.; Murg, V.; Cirac, J. I.; Verstraete, F. Matrix Product Operator Representations. *New J. Phys.* **2010**, *12*, 025012.
- (33) Haegeman, J.; Cirac, J. I.; Osborne, T. J.; Pizorn, I.; Vershelde, H.; Verstraete, F. Time-Dependent Variational Principle for Quantum Lattices. *Phys. Rev. Lett.* **2011**, *107*, 070601.
- (34) Haegeman, J.; Lubich, C.; Oseledets, I.; Vandereycken, B.; Verstraete, F. Unifying Time Evolution and Optimization with Matrix Product States. *Phys. Rev. B: Condens. Matter Mater. Phys.* **2016**, *94*, 165116.
- (35) Zaletel, M. P.; Mong, R. S. K.; Karrasch, C.; Moore, J. E.; Pollmann, F. Time-Evolving a Matrix Product State with Long-Ranged Interactions. *Phys. Rev. B: Condens. Matter Mater. Phys.* **2015**, *91*, 165112.
- (36) Dirac, P. A. M. Note on Exchange Phenomena in the Thomas Atom. *Math. Proc. Cambridge Philos. Soc.* **1930**, *26*, 376–385.
- (37) Langhoff, P. W.; Epstein, S. T.; Karplus, M. Aspects of Time-Dependent Perturbation Theory. *Rev. Mod. Phys.* **1972**, *44*, 602–644.
- (38) Chin, A. W.; Rivas, A.; Huelga, S. F.; Plenio, M. B. Exact Mapping between System-Reservoir Quantum Models and Semi-Infinite Discrete Chains Using Orthogonal Polynomials. *J. Math. Phys.* **2010**, *51*, 092109.
- (39) Prior, J.; Chin, A. W.; Huelga, S. F.; Plenio, M. B. Efficient Simulation of Strong System-Environment Interactions. *Phys. Rev. Lett.* **2010**, *105*, 050404.
- (40) Yao, Y. Coherent Dynamics of Singlet Fission Controlled by Nonlocal Electron-Phonon Coupling. *Phys. Rev. B: Condens. Matter Mater. Phys.* **2016**, *93*, 115426.
- (41) Yao, Y.; Xie, X.; Ma, H. Ultrafast Long-Range Charge Separation in Organic Photovoltaics: Promotion by Off-Diagonal Vibronic Couplings and Entropy Increase. *J. Phys. Chem. Lett.* **2016**, *7*, 4830–4835.
- (42) Kim, H. W.; Kelly, A.; Park, J. W.; Rhee, Y. M. All-Atom Semiclassical Dynamics Study of Quantum Coherence in Photosynthetic Fenna-Matthews-Olson Complex. *J. Am. Chem. Soc.* **2012**, *134*, 11640–11651.
- (43) Bai, S.-M.; Song, K.; Shi, Q. Effects of Different Quantum Coherence on the Pump-Probe Polarization Anisotropy of Photosynthetic Light-Harvesting Complexes: A Computational Study. *J. Phys. Chem. Lett.* **2015**, *6*, 1954–1960.
- (44) Tamura, H.; Huix-Rotllant, M.; Burghardt, I.; Olivier, Y.; Beljonne, D. First-Principles Quantum Dynamics of Singlet Fission: Coherent versus Thermally Activated Mechanisms Governed by Molecular π Stacking. *Phys. Rev. Lett.* **2015**, *115*, 107401.
- (45) Saller, M. A. C.; Habershon, S. Basis Set Generation for Quantum Dynamics Simulations Using Simple Trajectory-Based Methods. *J. Chem. Theory Comput.* **2015**, *11*, 8–16.
- (46) Tamura, H.; Burghardt, I.; Tsukada, M. Exciton Dissociation at Thiophene/Fullerene Interfaces: The Electronic Structures and Quantum Dynamics. *J. Phys. Chem. C* **2011**, *115*, 10205–10210.
- (47) Tamura, H.; Martinazzo, R.; Ruckebauer, M.; Burghardt, I. Quantum dynamics of ultrafast charge transfer at an oligothiophene-fullerene heterojunction. *J. Chem. Phys.* **2012**, *137*, 22A540.
- (48) Chenel, A.; Mangaud, E.; Burghardt, I.; Meier, C.; Desouter-Lecomte, M. Exciton dissociation at donor-acceptor heterojunctions: Dynamics using the collective effective mode representation of the spin-boson model. *J. Chem. Phys.* **2014**, *140*, 044104.
- (49) Mangaud, E.; Meier, C.; Desouter-Lecomte, M. Analysis of the non-Markovianity for electron transfer reactions in an oligothiophene-fullerene heterojunction. *Chem. Phys.* **2017**, *494*, 90–102.
- (50) Trotter, H. F. On the Product of Semi-Groups of Operators. *Proc. Am. Math. Soc.* **1959**, *10*, 545–551.
- (51) Suzuki, M. Generalized Trotter's Formula and Systematic Approximants of Exponential Operators and Inner Derivations with Applications to Many-Body Problems. *Commun. Math. Phys.* **1976**, *51*, 183–190.
- (52) Tamura, H.; Bittner, E. R.; Burghardt, I. Nonadiabatic quantum dynamics based on a hierarchical electron-phonon model: Exciton dissociation in semiconducting polymers. *J. Chem. Phys.* **2007**, *127*, 034706.
- (53) Gindensperger, E.; Cederbaum, L. S. Quantum dynamics in macrosystems with several coupled electronic states: Hierarchy of effective Hamiltonians. *J. Chem. Phys.* **2007**, *127*, 124107.
- (54) There is another applicable method for the transformation, which is to introduce the coupling to the vibrational bath via an effective coordinate; see, e.g.: Chernyak, V.; Mukamel, S. Collective coordinates for nuclear spectral densities in energy transfer and femtosecond spectroscopy of molecular aggregates. *J. Chem. Phys.* **1996**, *105*, 4565–4583.
- (55) Bulla, R.; Lee, H.; Tong, N.; Vojta, M. Numerical renormalization group for quantum impurities in a bosonic bath. *Phys. Rev. B: Condens. Matter Mater. Phys.* **2005**, *71*, 045122.
- (56) Kuzmich, A.; Padula, D.; Ma, H.; Troisi, A. Trends in the electronic and geometric structure of non-fullerene based acceptors for organic solar cells. *Energy Environ. Sci.* **2017**, *10*, 395–401.
- (57) Huynh, T. D.; Sun, K. W.; Gelin, M.; Zhao, Y. Polaron dynamics in two-dimensional photon-echo spectroscopy of molecular rings. *J. Chem. Phys.* **2013**, *139*, 104103.
- (58) Sun, K. W.; Gelin, M. F.; Chernyak, V.; Zhao, Y. Davydov Ansatz as an efficient tool for the simulation of nonlinear optical response of molecular aggregates. *J. Chem. Phys.* **2015**, *142*, 212448.
- (59) Mukamel, S. *Principles of Nonlinear Optical Spectroscopy*; Oxford University Press: New York, 1995.
- (60) Borrelli, R.; Gelin, M. F. Simulation of Quantum Dynamics of Excitonic Systems at Finite Temperature: an efficient method based on Thermo Field Dynamics. *Sci. Rep.* **2017**, *7*, 9127.